SUPERCONDUCTIVITY

Rapid change of superconductivity and electron-phonon coupling through critical doping in Bi-2212

Y. He[1,2]*, M. Hashimoto[3]*, D. Song[4]†, S.-D. Chen[1,2], J. He[1,2], I. M. Vishik[1]‡, B. Moritz[1,2], D.-H. Lee[5], N. Nagaosa[6], J. Zaanen[7], T. P. Devereaux[1,2], Y. Yoshida[4], H. Eisaki[4], D. H. Lu[3], Z.-X. Shen[1,2]§

Electron-boson coupling plays a key role in superconductivity for many systems. However, in copper-based high–critical temperature (T_c) superconductors, its relation to superconductivity remains controversial despite strong spectroscopic fingerprints. In this study, we used angle-resolved photoemission spectroscopy to find a pronounced correlation between the superconducting gap and the bosonic coupling strength near the Brillouin zone boundary in $Bi_2Sr_2CaCu_2O_{8+\delta}$. The bosonic coupling strength rapidly increases from the overdoped Fermi liquid regime to the optimally doped strange metal, concomitant with the quadrupled superconducting gap and the doubled gap-to-T_c ratio across the pseudogap boundary. This synchronized lattice and electronic response suggests that the effects of electronic interaction and the electron-phonon coupling (EPC) reinforce each other in a positive-feedback loop upon entering the strange-metal regime, which in turn drives a stronger superconductivity.

The phase diagram of cuprate high-temperature superconductors hosts a number of complex orders, types of fluctuations, and interactions (*1*–*4*). In the non–Fermi liquid strange-metal regime, a hierarchy of microscopic interactions are intimately at play but not fully understood (*1*, *2*, *4*). Although the experimental evidence for d-wave superconductivity (*5*–*7*) naturally points to an electron-electron interaction–based pairing mechanism (*8*–*12*), the omnipresent charge order (*3*) points to the role of electron-phonon coupling (EPC), especially in the context of enhanced EPC by electronic correlation (*13*, *14*) and multichannel boosted superconductivity (*15*–*17*). Although there have been reports of EPC imprinting on the electronic structure of many cuprate superconductors (*18*–*21*), little evidence directly correlates EPC with the intertwined orders in the phase diagram (*1*, *2*). By focusing on the overdoped side in $Bi_2Sr_2CaCu_2O_{8+\delta}$ (Bi-2212), we used angle-resolved photoemission spectroscopy (ARPES) to uncover a set of pronounced effects rapidly crossing over from the overdoped Fermi liquid regime to the optimally doped strange metal, closely associated with the putative pseudogap quantum critical point.

To understand the doping dependence of the superconducting character, we first investigated the energy gap. Figure 1A depicts the recently proposed phase diagram, with an emphasis on the pseudogap phase boundary (red boxed area) (*22*, *23*). In this doping range, the system is marked by a strange-metal normal state characterized by spectral incoherence and linear resistivity at high temperatures (*2*), followed by intertwined states with pseudogap and superconductivity at low temperatures (*23*). Figure 1B plots the Fermi-Dirac function divided energy distribution curves (FD-EDCs) at the antinodal Fermi momentum k_F from hole doping (per Cu atom) p = 0.14 [underdoped critical temperature (T_c) = 92 K, UD92] to p = 0.24 (overdoped T_c = 47 K, OD47), for both low temperatures (blue; $T << T_c$) and high temperatures [red; $T \sim T^*$ (where T^* is the pseudogap temperature) for pseudogap regime, $T > T_c$ for nonpseudogap regime, generally referred to as $T >> T_c$ hereafter (*24*)]. The spectra in the deeply overdoped region are characterized by prominent Bogoliubov quasiparticle peaks at low temperature ($T << T_c$) and pronounced coherent peaks in the normal state ($T >> T_c$). The extracted antinodal gap size Δ_{AN} at $T << T_c$ is plotted as a function of the superconducting transition temperature in Fig. 1C, revealing a fourfold change in contrast to the only twofold change in T_c across the doping range of interest. The gap-to-T_c ratio reaches the weak coupling d-wave Bardeen-Cooper-Schrieffer (BCS) value in the doping range where $T_c \lesssim 65$K [lower dashed line at $2\Delta/k_BT_c$ = 4.3 (where k_B is the Boltzmann constant)], and the scattering dynamics can be described by Fermi liquid theory (fig. S2). Figure 1D shows the doping dependence of the gap-to-T_c ratio $2\Delta/k_BT_c$, which rapidly increases from ~4.3 at $p \sim 0.22$, a doping where $T_c \sim T^*$ (*22*, *23*), to ~10 at $p \sim 0.19$, a doping where a pseudogap critical point has been suggested (*2*, *25*). In this rapid process of the superconducting character change, T_c rises from 65 to 95 K despite the increasing presence of the competing pseudogap (*23*). Throughout this doping range, the low-temperature spectral gap takes the d-wave form, which means that the antinodal gap size Δ_{AN} embodies the entire d component (also known as the nodal gap Δ_N) in this discussion (fig. S3) (*22*, *24*). This doping range is to be distinguished from the underdoped region, where the energy gap deviates from the d-wave form (*4*, *22*). Indeed, Δ_{AN} and Δ_N show consistent behavior (Fig. 1, C and D).

With the rapid doping evolution of the superconducting character, the EPC around the Brillouin zone (BZ) boundary also undergoes a substantial change. Figure 2A shows the FD-EDCs from (π, 0), where the peak directly reflects the antinodal band bottom (high temperatures, red), and the spectral minima in the "peak-dip-hump" structure are minimally disturbed by the bonding band (low temperatures, blue) (*24*). Such spectral dips are commonly interpreted as the fingerprint of electron-boson coupling and become prominent with strong EPC (*16*, *18*, *24*, *26*). This is inferred from the variation with doping of the difference between low- and high-temperature spectra (highlighted in gray); the spectral weight of this difference increases with growing EPC (Fig. 2B and fig. S4). Note that the effect of the weakly temperature dependent bilayer splitting is minimized with this analysis (*24*). As shown in Fig. 2D and fig. S6B, the dip position tracks the rapid evolution of Δ_{AN} at $T << T_c$ by an energy offset of ~37 meV, which is nearly independent of doping, agrees well with the energy of the B_{1g} oxygen bond-buckling phonon mode (*18*, *24*), and is qualitatively consistent with previous scanning tunneling microscope studies (*20*). Such a mode was also revealed in recent high-resolution photoemission studies on similarly overdoped systems near the antinode (*27*). Surprisingly, the spectral weight associated with the dip, which reflects the EPC strength (*24*), abruptly grows between $p \sim 0.22$ and 0.19 (Fig. 2E). This finding, along with the similar behavior in doping-dependent charge-transport properties (*28*), cannot be explained by a simple chemical potential shift, which has yet to cross the band bottom at (π, 0) (Fig. 2A). For comparison, the predepletion of the density of states (DOS) from the high-temperature normal state to T_c (ratio between the red and blue arrows in Fig. 2C; also see fig. S6C) is plotted in Fig. 2F. Compared with the conventionally used T^* or Δ_{AN}, this quantity better disentangles the pseudogap contribution from the bulk superconductivity, reflecting the direct DOS depletion effects dominated by the pseudogap. Clearly, all three quantities—superconductivity (Fig. 2D), pseudogap (Fig. 2F), and EPC strength (Fig. 2E)—show concomitant onset and rapid change in the interval p = 0.19 to 0.22 in a highly correlated fashion.

[1]Geballe Laboratory for Advanced Materials, Departments of Physics and Applied Physics, Stanford University, Stanford, CA 94305, USA. [2]SIMES, SLAC National Accelerator Laboratory, Menlo Park, CA 94025, USA. [3]Stanford Synchrotron Radiation Lightsource, SLAC National Accelerator Laboratory, Menlo Park, CA 94025, USA. [4]National Institute of Advanced Industrial Science and Technology, Tsukuba 305-8568, Japan. [5]Department of Physics, University of California, Berkeley, CA 94720, USA. [6]Quantum-Phase Electronics Center, Department of Applied Physics, University of Tokyo, Tokyo 113-8656, Japan. [7]Instituut-Lorentz for Theoretical Physics, Leiden University, Leiden, Netherlands.
*These authors contributed equally to this work. †Present address: Department of Physics and Astronomy, Seoul National University, Seoul 08826, Republic of Korea. ‡Present address: Department of Physics, University of California, Davis, CA 95616, USA.
§Corresponding author. Email: zxshen@stanford.edu

By showing plots of integrated spectra near the antinode, Figure 2C highlights the marked contrast between the two distinct regimes: the complex strange-metal regime near optimal doping (C1; strong pairing, strong EPC, and pseudogap) and the deeply overdoped region, in which the system behavior appears to submit to the classic BCS rules (C2; weaker pairing, weaker EPC, and no pseudogap). The contrast in the spectra is most pronounced in the normal state where no quasiparticles exist in the strange-metal state, but Fermi liquid quasiparticles are apparent in the deeply overdoped regime. The main discovery is that the strange-metal phase involves not only strong correlations and incipient intertwining electronic orders but also lattice degree of freedom (in particular, the B_{1g} phonon for this system). The peak-dip-hump structure is the low-temperature remnant of such intertwinement (after superconductivity has already set in) and is largely smeared out at high temperatures by the spectral incoherence characteristic of the strange-metal state.

On the basis of the doping-dependent investigation (Fig. 2, D to F), we suggest that the increasing electronic correlation, marked by the entrance into the strange-metal regime and the emergence of pseudogap, may have triggered this sudden EPC enhancement and the complex feedback interaction that follows. It is

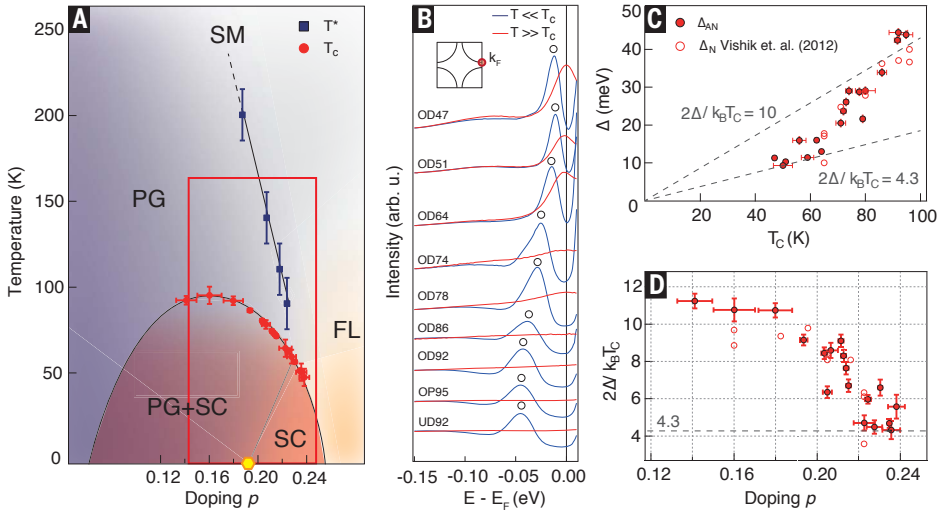

Fig. 1. Superconductivity rapidly deviates from the weakly coupled d-wave BCS limit with underdoping. (**A**) Schematic phase diagram for Bi-2212 [reproduced from (*22*)], with an emphasis on the doping range of interest (boxed in red). Blue squares represent the antinodal gap-opening temperature T^*; red circles denote the superconducting transition temperature T_c (fig. S1). PG, pseudogap; SC, superconductivity; SM, strange metal; FL, Fermi liquid. (**B**) FD-EDCs taken at the antinodal k_F for a series of doping. Red curves refer to $T \sim T^*$ for $p < 0.22$ and $T > T_c$ for $p > 0.22$, and blue curves indicate $T << T_c$ for all dopings (*24*). Black circles denote the superconducting quasiparticle peak position. The inset schematically illustrates the momenta of the listed spectra. arb. u., arbitrary units; E, energy; E_F, Fermi energy. (**C**) Antinodal gap Δ_{AN} (solid circles) and nodal gap Δ_N (open circles) (*22*) plotted against the sample T_c. The two dashed lines mark the gap-to-T_c ratios of 4.3 (the weakly coupled d-wave BCS value) and 10. (**D**) The gap-to-T_c ratio shows a rapid deviation from 4.3 (horizontal black dashed line) at $p < 0.22$. In (A), (C), and (D), error bars are propagated from T_c uncertainties (see fig. S1).

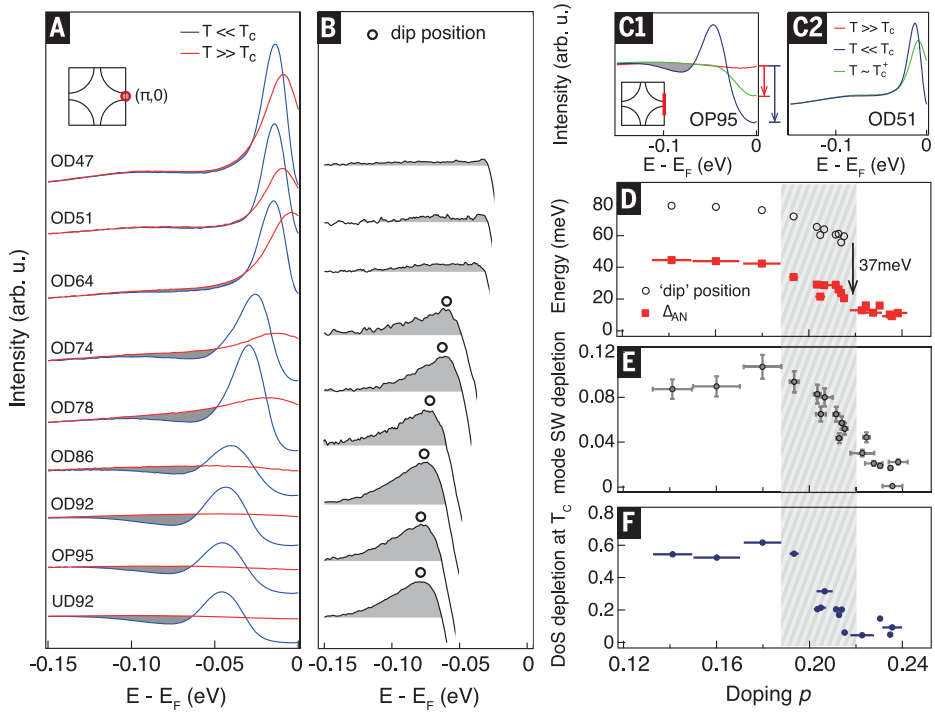

Fig. 2. Abrupt growth of the EPC strength with underdoping. (**A**) The (π, 0) FD-EDCs taken at low temperature (blue) and high temperature (red, $T \sim T^*$ for pseudogap regime, $T > T_c$ for sufficiently overdoped regime) from heavy overdoping (OD47) to slight underdoping (UD92). (**B**) Spectral intensity difference between the two temperatures for each doping. Black circles denote the dip maxima. (**C**) Integrated FD-EDC over the antinodal momenta at low temperatures ($T << T_c$, blue), just above T_c ($T \sim T_c^+$, green), and high temperatures ($T >> T_c$, red) for the $p = 0.16$ sample (OP95, C1) and the $p = 0.23$ sample (OD51, C2). The momentum integration range is noted by the red bar in the inset schematic BZ. The spectra are normalized to the total spectral weight between binding energies of 200 and 300 meV. (**D**) Doping-dependent dip position and coevolving antinodal gap Δ_{AN}. (**E**) Doping-dependent spectral weight (SW) of the dip [gray area in (B)] relative to the total spectral weight of the normal state. (**F**) Doping-dependent antinodal spectral weight depletion at T_c^+ (red arrow in C1) relative to the full depletion at $T << T_c$ (blue arrow in C1), derived from the intensity of the integrated FD-EDCs within ±2 meV of E_F. In (D) to (F), error bars are propagated from T_c uncertainties (see fig. S1).

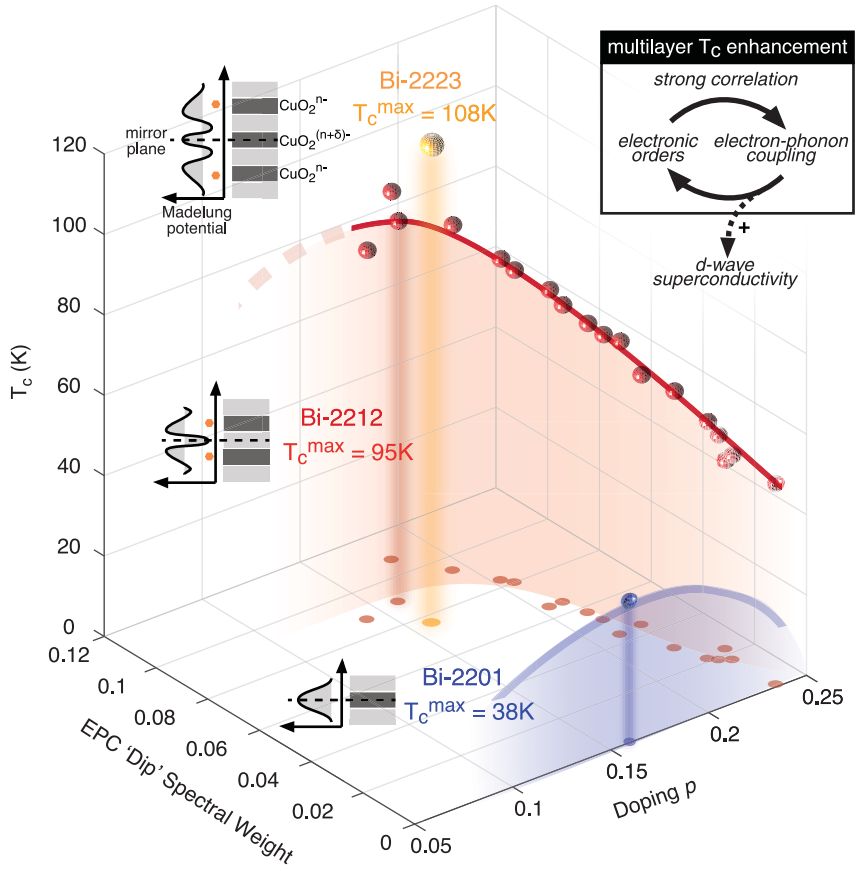

Fig. 3. Intertwined growth of superconductivity and EPC tuned by the hole concentration. The red line is an illustration of the T_c in Bi-2212 (T_c^{max} = 95 K). The blue shaded region and line represent the single-layer Bi-2201 system, in which the coupling to the B_{1g} mode is weak and T_c^{max} is only 38 K. The yellow ball represents the optimally doped trilayer Bi-2223, in which T_c^{max} is 108 K. The top-right inset shows the intertwined relation between the pseudogap and the EPC under strong electronic correlation. The Madelung potential and the lattice stacking along the *c* axis are schematically depicted for the single-layer, bilayer, and trilayer systems (left insets). The dark gray blocks represent the CuO_2^{n-} plane, and the light gray blocks represent the charge reservoir layers (Ca^{2+}, SrO, BiO^+). The orange circles mark the CuO_2^{n-} planes that experience to the first order a nonzero out-of-plane electric field.

likely that between p = 0.22 and 0.19 the charge carriers slow down, the charge screening becomes inoperative, and the strange metal takes over (also see fig. S8). With further underdoping and stronger pairing, EPC and the pseudogap become closely tied phenomena (Fig. 3, top right inset). Although the electronically driven charge density wave (CDW) does not result in substantial static lattice deformation, the "dynamical" effects of EPC—giant phonon anomalies (*29*), the large sensitivity of the charge order and superfluid density to isotope substitution (*19*), as well as the strengthening of the superconductivity caused by phonon pumping (*30*)—are indeed abundant in the underdoped region. Our present results indicate that the non–Fermi liquid nature of the strange metal appears to have a drastic impact on the fundamental physics of the EPC, which may well be at the origin of these highly anomalous EPC effects on the intertwined orders at low temperatures (*31*). Consequently, EPC and strange-metal physics play together to enhance the system's tendency to order, inducing instability that leads to CDW or more complex electronic textures (*3*). Further underdoping leads to extreme EPC amplified by correlation effects, where the charge carriers eventually develop polaronic signatures (*13*). In particular, the B_{1g} phonon is suggested to accommodate the d-wave form factor of both the CDW (particle-hole channel) and the superconductivity (particle-particle channel) in the cuprate systems, providing pathways for the lattice to interact with the electronic orders (*32*).

Indeed, the pseudogap temperature T^* near optimal doping receives a notable increase from single-layer to bilayer Bi-based cuprate systems (fig. S8C). Only in the multilayer case does the oxygen B_{1g} mode substantially couple to electrons: As the CuO_2^{n-} planes do not lie on a crystal mirror plane, a coupling can only arise from first-order *c* axis atomic displacements (Fig. 3, left insets). Such layer dependence also holds when the trilayer system is taken into account (*33*). Therefore with underdoping, the rapid formation of the pseudogap and enhanced EPC could be perceived as a result of a positive feedback under increasing electronic correlation, which efficiently reinforces the system's already strong tendency to order.

More intriguingly, superconductivity may benefit from this feedback loop. Figure 3 compiles the superconducting T_c of the single-layer (Bi-2201, blue), bilayer (Bi-2212, red), and trilayer (Bi-2223, yellow) systems as a function of doping and antinodal EPC dip strength. The maximum T_c sees a considerable increase from single-layer to multilayer systems. Although the growing electronic correlation strength from the overdoped regime toward the optimal doping may have strengthened the pseudogap (*1*–*4*), it also joins efforts with the enhanced EPC to achieve the higher T_c in multilayer cuprate superconductors than in their single-layer counterparts (*33*). As a corroborative example, a recent photoemission study on a monolayer FeSe film system demonstrated the experimental viability to have a secondary phononic channel as the superconductivity enhancer (*16*), boosting T_c by as much as 50% in comparison with the uncoupled case. The oxygen bond-buckling B_{1g} phonon couples strongly in the multilayer cuprates, owing to the steep Madelung potential going through the CuO_2^{n-} planes that do not constitute the crystal mirror plane (Fig. 3, left insets, orange circles). This phonon mode is also known to favor scattering with small momentum transfer, owing to its preferential coupling to electrons in the antinodal region, and is inherently poised for d-wave superconductivity enhancement (*15*). This complex involvement of EPC in the pairing process may also be the underlying reason for the dynamical and diverse manifestation of isotope effects (*19*, *20*). Therefore, it may be insufficient to regard Cooper pairing as driven by pure electron-electron interactions in the optimal and underdoped regions.

On the other hand, the deeply overdoped regime emerges as a weakly coupled, simpler superconductor with a respectably high T_c in excess of 50 K, which offers a cleaner platform to investigate the pairing mechanism. Meanwhile, with enhanced correlation in the strange-metal regime, EPC and the intertwined electronic orders form a positive-feedback loop (Fig. 3, right inset, solid arrows) that ultimately provides an

additional pathway for T_c enhancement by EPC in the multilayer systems (dashed arrow). From a broader perspective, cuprate superconductors, given this interpretation of their rich phase diagram, may be generalized as a new model system for testing EPC-enhanced superconductivity through multiple underlying channels. Systematic investigation of the B_{1g} phonon self energy around the critical doping via various scattering techniques may provide valuable insights into such scenarios.

REFERENCES AND NOTES

1. E. Fradkin, S. A. Kivelson, J. M. Tranquada, *Rev. Mod. Phys.* **87**, 457–482 (2015).
2. B. Keimer, S. A. Kivelson, M. R. Norman, S. Uchida, J. Zaanen, *Nature* **518**, 179–186 (2015).
3. R. Comin, A. Damascelli, *Annu. Rev. Condens. Matter Phys.* **7**, 369–405 (2016).
4. M. Hashimoto, I. M. Vishik, R. H. He, T. P. Devereaux, Z.-X. Shen, *Nat. Phys.* **10**, 483–495 (2014).
5. W. N. Hardy, D. A. Bonn, D. C. Morgan, R. Liang, K. Zhang, *Phys. Rev. Lett.* **70**, 3999–4002 (1993).
6. Z. Shen *et al*., *Phys. Rev. Lett.* **70**, 1553–1556 (1993).
7. D. A. Wollman, D. J. Van Harlingen, W. C. Lee, D. M. Ginsberg, A. J. Leggett, *Phys. Rev. Lett.* **71**, 2134–2137 (1993).
8. D. J. Scalapino, E. Loh Jr., J. E. Hirsch, *Phys. Rev. B* **34**, 8190–8192 (1986).
9. G. Baskaran, Z. Zou, P. W. Anderson, *Solid State Commun.* **63**, 973–976 (1987).
10. G. Kotliar, J. Liu, *Phys. Rev. B* **38**, 5142–5145 (1988).
11. P. A. Lee, N. Nagaosa, X.-G. Wen, *Rev. Mod. Phys.* **78**, 17–85 (2006).
12. P. Monthoux, D. Pines, G. G. Lonzarich, *Nature* **450**, 1177–1183 (2007).
13. A. S. Mishchenko, N. Nagaosa, *Phys. Rev. Lett.* **93**, 036402 (2004).
14. S. Gerber *et al*., *Science* **357**, 71–75 (2017).
15. S. Johnston *et al*., *Phys. Rev. B* **82**, 064513 (2010).
16. J. J. Lee *et al*., *Nature* **515**, 245–248 (2014).
17. Z.-X. Li, F. Wang, H. Yao, D.-H. Lee, *Sci. Bull.* **61**, 925–930 (2016).
18. T. Cuk *et al*., *Phys. Stat. Sol. B* **242**, 11–29 (2005).
19. J. L. Tallon, R. S. Islam, J. Storey, G. V. M. Williams, J. R. Cooper, *Phys. Rev. Lett.* **94**, 237002 (2005).
20. J. Lee *et al*., *Nature* **442**, 546–550 (2006).
21. H. Anzai *et al*., *Sci. Rep.* **7**, 4830 (2017).
22. I. M. Vishik *et al*., *Proc. Natl. Acad. Sci. U.S.A.* **109**, 18332–18337 (2012).
23. M. Hashimoto *et al*., *Nat. Mater.* **14**, 37–42 (2015).
24. Materials and methods are available as supplementary materials.
25. S. Sachdev, *Phys. Stat. Sol. B* **247**, 537–543 (2010).
26. D. J. Scalapino, J. R. Schrieffer, J. W. Wilkins, *Phys. Rev.* **148**, 263–279 (1966).
27. J. He, in *Angle-Resolved Photoemission Spectroscopy on High-Temperature Superconductors: Studies of Bi-2212 and Single-Layer FeSe Film Grown on $SrTiO_3$ Substrate* (Springer, 2016), pp. 71–79.
28. Y. Ando, Y. Kurita, S. Komiya, S. Ono, K. Segawa, *Phys. Rev. Lett.* **92**, 197001 (2004).
29. M. Le Tacon *et al*., *Nat. Phys.* **10**, 52–58 (2014).
30. R. Mankowsky *et al*., *Nature* **516**, 71–73 (2014).
31. J. Zaanen, Y. Liu, Y.-W. Sun, K. Schalm, in *Holographic Duality in Condensed Matter Physics* (Cambridge Univ. Press, 2015), chap. 2.
32. C. Honerkamp, H. C. Fu, D.-H. Lee, *Phys. Rev. B* **75**, 014503 (2007).
33. T. Sato *et al*., *Phys. Rev. Lett.* **89**, 067005 (2002).

ACKNOWLEDGMENTS

We thank R. Hackl, S. Kivelson, S.-L. Yang, M. Yi, Y. Wang, and E. W. Huang for discussions. ARPES experiments were performed at Stanford Synchrotron Radiation Lightsource, SLAC National Accelerator Laboratory, and at Stanford Geballe Laboratory for Advanced Materials at Stanford University. **Funding:** This study is supported by the U.S. Department of Energy (DOE), Office of Science, Office of Basic Energy Sciences, Division of Materials Sciences and Engineering, under contract DE-AC02-76SF00515. D.H.L. was supported by the DOE, Office of Science, Office of Basic Energy Sciences, Division of Materials Sciences and Engineering, under grant DE-AC02-05CH11231. **Author contributions:** Conceptualization and writing: Z.-X.S., Y.H., M.H., B.M., S.-D.C., D.-H.L., N.N., J.Z., and T.P.D.; investigation and analysis: Y.H, M.H., S.D.C., J.H., and I.M.V; methodology and software: Y.H., B.M., and T.P.D.; resources: M.H., D.-H.L., D.S., Y.Y., and H.E. **Competing interests:** The authors declare no competing interests. **Data and materials availability:** All data are present in the paper or the supplementary materials and are available in tab-delimited file format (.rar) in the supplementary data files.

SUPPLEMENTARY MATERIALS

www.sciencemag.org/content/362/6410/62/suppl/DC1
Materials and Methods
Supplementary Text
Figs. S1 to S9
Table S1
References (*34*–*51*)
Data Files

27 October 2017; accepted 30 July 2018
10.1126/science.aar3394

Rapid change of superconductivity and electron-phonon coupling through critical doping in Bi-2212

Y. He, M. Hashimoto, D. Song, S.-D. Chen, J. He, I. M. Vishik, B. Moritz, D.-H. Lee, N. Nagaosa, J. Zaanen, T. P. Devereaux, Y. Yoshida, H. Eisaki, D. H. Lu and Z.-X. Shen

Science **362** (6410), 62-65.
DOI: 10.1126/science.aar3394

Conspiring interactions in a cuprate

More than 30 years after the discovery of high-temperature superconductivity in copper oxides, its mechanism remains a mystery. Electron pairing mediated solely by lattice vibrations—phonons—is thought to be insufficient to account for the high transition temperatures. He *et al.* found a rapid and correlated increase of the superconducting gap and electron-phonon interactions as the chemical composition of their bismuth-based cuprate samples was varied across a critical doping concentration. The interplay of electron-phonon with electron-electron interactions may lead to enhanced transition temperatures.

Science, this issue p. 62